Voltage Fluctuation to Current Converter with Coulomb-Coupled Quantum Dots

F. Hartmann,[1,*] P. Pfeffer,[1] S. Höfling,[1,2] M. Kamp,[1] and L. Worschech[1]

[1]*Technische Physik, Universität Würzburg, Physikalisches Institut and Wilhelm Conrad Röntgen Research Center for Complex
Material Systems, Am Hubland, D-97074 Würzburg, Germany*
[2]*SUPA, School of Physics and Astronomy, University of St. Andrews, St. Andrews, KY16 9SS, United Kingdom*

We study the rectification of voltage fluctuations in a system consisting of two Coulomb-coupled quantum dots. The first quantum dot is connected to a reservoir where voltage fluctuations are supplied and the second one is attached to two separate leads via asymmetric and energy-dependent transport barriers. We observe a rectified output current through the second quantum dot depending quadratically on the noise amplitude supplied to the other Coulomb-coupled quantum dot. The current magnitude and direction can be switched by external gates, and maximum output currents are found in the nA region. The rectification delivers output powers in the pW region. Future devices derived from our sample may be applied for energy harvesting on the nanoscale beneficial for autonomous and energy-efficient electronic applications.

Extracting work from random fluctuations by energy conversion to a unidirectional particle flow is a key enabling technology and has consequently triggered substantial experimental and theoretical work [1–4]. The exploitation of temperature and fluctuation gradients for energy harvesting has led to new concepts such as Brownian and Büttiker-Landauer motors [5–8], phonon rectifiers [9,10], and piezoelectric nanogenerators [11–13]. Challenging factors in miniaturizing heat engines are an efficient energy conversion and the maintenance of well-defined hot and cold spots [14]. Quantum dot structures are among the smallest possible heat engines conceived thus far. Pioneering work in this field was conducted by, among others, Molenkamp *et al.*, who measured the Seebeck voltage of single quantum dots (QDs) and quantum point contacts (QPCs) [15–17]. In recent years, research concerning heat engines based on QDs and QPCs followed [18–22]. Furthermore, Coulomb-coupled systems attracted attention due to their ability to generate currents in unbiased wires via the Coulomb drag [23–25]. A striking proposal combining rectifying effects with QDs was recently made by Sánchez *et al.*, who showed that two capacitively coupled QDs connected to electron reservoirs operated in the Coulomb-blockade regime can act as a rectifier that transfers each energy quantum that passes from one to the other QD to the motion of single electrons (i.e., to charge quanta) [26]. Notably, the heat and charge current directions are decoupled in the proposed system. Later, Sothmann *et al.* investigated a similar design based on open QD systems (with conductances higher than the conductance quantum) exhibiting higher output currents, which makes this proposal more accessible to experimental realization [27,28]. Furthermore, it combines maximum output power as well as maximum efficiency at the same electrostatic configuration, which is in contrast to

Coulomb-blockade systems, where maximum efficiency theoretically occurs at zero output power [26].

In this Letter, we present a system that converts voltage fluctuations into a directed current depending on the fluctuation's amplitude and whose direction and magnitude can be manipulated via external gates.

The operation principle of the device is illustrated in Fig. 1(a) where the upper QD_t is represented as the cavity
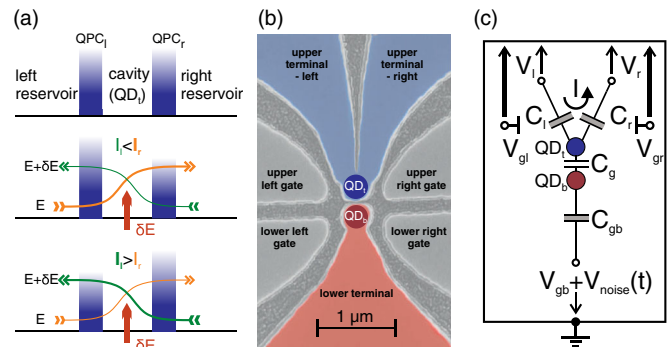

FIG. 1 (color online).   (a) Schematic operating principle. Top: Designation of system components. Center: Asymmetric configuration with charge current flow to the right. Bottom: Asymmetric configuration with charge current flow to the left. For details see main text. (b) Electron microscopy image of the sample. The top, current carrying part of the system is shaded in blue, the bottom part, where the voltage fluctuations are supplied, in red. The respective QDs QD_t and QD_b are highlighted in dark blue and dark red. (c) Equivalent circuit with corresponding capacitances. The current through the upper part is measured via a picoamperemeter. The two upper side gates and their voltages V_{gl} and V_{gr} control the conductances of the left and right channel, whereas V_{gb} influences both channels almost equally and shifts the QD's energy levels. V_{noise} can be added to V_{gb} and provides the fluctuations which the device is able to rectify.

connected via QPCs to electron reservoirs. The lower QD_b serves as the energy source, which is mediated via Coulomb interaction to electrons in QD_t, thus raising their energy by δE. The two blue columns in the sketch represent the transmissivities of the two QPCs. The brighter the part of a blue column, the higher the transmissivity at the respective energy. Horizontal arrows illustrate the current flow through QD_t with bigger arrows symbolizing higher currents. Vertical arrows stand for the energy supply δE to the upper cavity QD_t. Provided that the whole electron path [thicker orange arrow in the middle panel of Fig. 1(a)] for electrons entering the cavity from the left with a lower energy, then increasing their energy by δE in the cavity, and finally leaving the cavity through the right QPC has a larger total transmissivity compared to electron path with the opposite direction (thin green arrow), QD_t operates as the rectifier. By changing the transmissivities by external gates or a proper asymmetric design of the QPCs, the rectified current direction can be inverted (lower panel). In this device concept, no current flows between the energy supplying QD_b and the rectifier QD_t.

For the realization of such structures, we grew a modulation doped GaAs/AlGaAs heterostructure with a high mobility two-dimensional electron gas (2DEG) located about 80 nm below the surface by molecular beam epitaxy. Electron beam lithography and dry chemical etching techniques were used to etch trenches that cut through the 2DEG, defining the device and also outer side gates. Figure 1(b) shows an electron microscopy image of such a sample. For clarity, QD_t connected to the left and right upper terminals is dyed in blue. QD_b connected to the lower terminal is dyed in red. The upper left and right gates were used to control the transmittivities of the QD_t's contacts with the applied gate voltages V_{gl} and V_{gr}. The lower gates were directly connected to ground. QD_t is connected to the left and right voltage sources with voltages V_l and V_r, respectively. QD_b is connected to the lower reservoir where controllable voltage fluctuations due to a noise source occur. Figure 1(c) shows the equivalent circuit.

Similar to a Smoluchowski-Feynman ratchet [14], the analyzed converter can only work when the magnitude of fluctuations differs across the device, meaning in our case, when the fluctuations in QD_b exceed those in the left and right reservoir. In order to prevent particle exchange between the two subsystems, we separated them using etched trenches of about 150 nm. Thus, electronic fluctuations in QD_b are mostly conveyed to the upper subsystem by means of Coulomb coupling to QD_t.

Figure 1(c) depicts the circuit diagram of the device. The QDs are coupled to their respective reservoirs by leads, whereas the QDs are coupled to each other by means of the capacitance C_g. The upper reservoirs can be biased by $V_{lr} = V_l - V_r$, and the current through the contacts was measured using a low noise picoamperemeter. The bottom QD can serve as local gate of QD_t by tuning the voltage
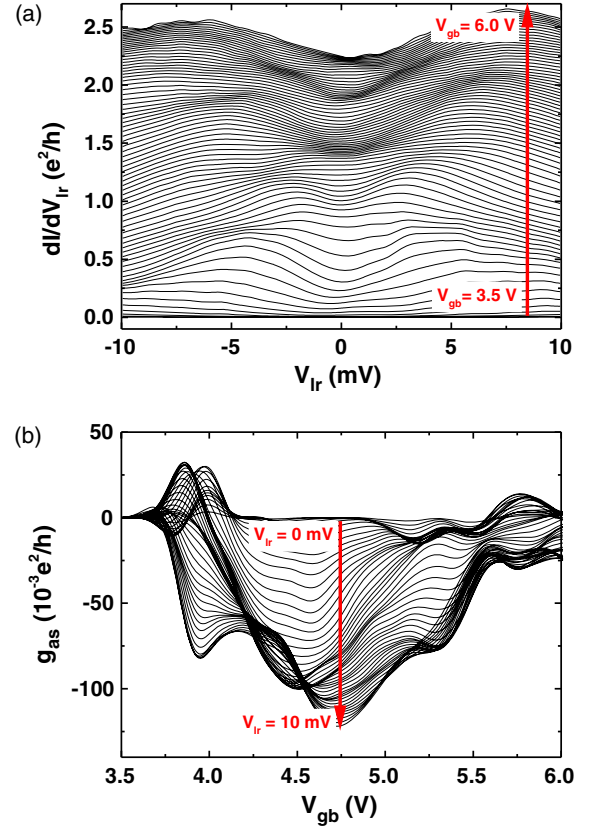

FIG. 2 (color online). (a) Differential conductance traces for V_{gb} from 3.5 to 6 V against V_{lr}. Dark regions where the traces lie close to each other signify stable conductances. (b) Conductance asymmetry g_{as} against V_{gb} for V_{lr} ranging from 0 to 10 mV.

V_{gb}. All experiments reported here were conducted at 4.2 K in the dark by immersing the sample in liquid helium.

Figure 2(a) shows several conductance traces dI/dV_{lr}, with I being the current through QD_t for different V_{gb} ranging from 3.5 to 6 V while $V_{gl} = V_{gr} = 0$ V. One can see several darker regions of a high trace density where the conductance is relatively stable against gate voltage changes. For small bias voltages the conductance at $V_{gb} = 4.7$ V lies inside a stable region reaching a value of about $1.5e^2/h$.

For the purpose of observing the upper system part's ability to rectify fluctuating currents, it is useful to define the conductance asymmetry

$$g_{as}(V_{lr}) = 1/2[dI/dV_{lr}(-V_{lr}) - dI/dV_{lr}(+V_{lr})], \quad (1)$$

which is displayed in Fig. 2(b) versus V_{gb} (different traces). Varying V_{gb} from small to higher values shifts the system from a configuration with small and sign-changing g_{as} values to a region exhibiting large negative g_{as} when $V_{gb} \approx 4.7$ V. For even larger V_{gb}, small and sign-changing g_{as} can be seen again. Large positive or negative values of g_{as} reflect transmission asymmetries and can be found in

the region between $V_{gb} = 3.8$ and 5.5 V. Thus, the operating point was set to this open QD regime at $V_{gb} = 4.7$ V in the following experiment.

For the controlled generation of voltage fluctuations in the lower reservoir, a Gaussian-distributed and spectrally flat noise source with a root mean square noise amplitude σ_{noise} and a cutoff frequency $f = 20$ MHz was used. The noise was added to the static gate voltage V_{gb} resulting in an overall voltage at the lower reservoir of $V_{ov}(t) = V_{gb} + V_{noise}(t)$. In order to keep the central electrostatic potential of QD_t constant while asymmetrically controlling the conductances of the left and right channel G_l and G_r (reducing G_l increases G_r and vice versa), V_{gl} and V_{gr} were varied in push-pull configuration, i.e., $\Delta V_{gl} = -\Delta V_{gr}$, with $V_{gl} + V_{gr} = 0$ in our case. In Fig. 3(a) the rectified current through QD_t is plotted for different noise amplitudes ranging from $\sigma_{noise} = 7.6$ to 144 mV for $V_{lr} = 0$ V. At zero σ_{noise}, no rectified current I could be measured, but applying noise and sweeping the side gate voltages allows detection and control of the current flow. Starting with a gate voltage configuration of $V_{gl} = -V_{gr} = -2$ V and increasing $\Delta V_{gl} = -\Delta V_{gr}$ initially increases the current from zero to a maximal value

that depends on the applied noise. Thereafter, I decreases again and vanishes completely at around $V_{gl} = 0.01$ V (independently of σ_{noise}). At $V_{gl} = V_{gr} = 0$, currents of up to 10 nA can be measured, which indicates that also via a proper asymmetric design of QD_t contacts a rectified current can be generated and thus side gates for application of an in-plane electric field are, in principle, not necessary to achieve rectification. A further increase of V_{gl} changes the current direction. I, therefore, becomes negative, reaches a minimum, and finally increases back to zero again. The disappearance of I below and above certain side gate configurations can be understood bearing in mind that the push-pull method closes one channel while opening the other one [29]. The insets of Fig. 3(a) present the maximum currents for both directions in dependence on the noise amplitude σ_{noise}.

A simulated model of the rectification currents after Eqs. (4) and (5) in Ref. [27] can be seen in Fig. 3(b). The theoretical curves shown there have been modeled using the following relations and demonstrate the inversion of the critical rectification parameter Λ by changing the gate voltages V_i ($i = gr, gl$, left and right side gate) in push-pull fashion. According to Ref. [27], the rectified current I through the upper quantum dot system can be expressed as

$$ I = \frac{\Lambda}{\tau_{RC}} k_B \Delta T. \quad (2) $$

Here, ΔT denotes the temperature difference between the upper quantum dot system at temperature T_C (cold) and the bottom quantum dot system at temperature T_H (hot), k_B is the Boltzmann constant, τ_{RC} is the effective RC time of the (double) cavity with the effective capacitance C_{eff} and conductance G_{eff} (cf. Ref. [27]). We assume that the energy difference $k_B \Delta T$ between the two systems equals the energy stored on the capacitor E_{cap}, with $E_{cap} = 1/2 C_g \sigma_{noise}^2$ (C_g being the capacitance between the two QDs). Thus,

$$ I = 1/2 \Lambda C_g / C_{eff} G_{eff} \sigma_{noise}^2. \quad (3) $$

The rectification parameter Λ can be written in terms of energy-independent parts $G_i = (e^2/h)T_i$, with transmission T_i, and energy-dependent parts $G_i' = (e^3/h)T_i'$, with transmission T_i'. Following Ref. [30], the energy-dependent conductance of a QPC is

$$ G(E_n, T) = \frac{e^2}{h} \sum_{n=1}^{\infty} \left[1 + \exp\left(\frac{E_n - E_F}{k_B T}\right) \right]^{-1}, \quad (4) $$

where E_F is the Fermi energy, E_n the energy of the bottom of the nth subband, and T the temperature. We model the conductance of each channel via Eq. (4), where $E_F - E_n = e\eta_i V_i$, $i = gl$ or $i = gr$, and η_i corresponds
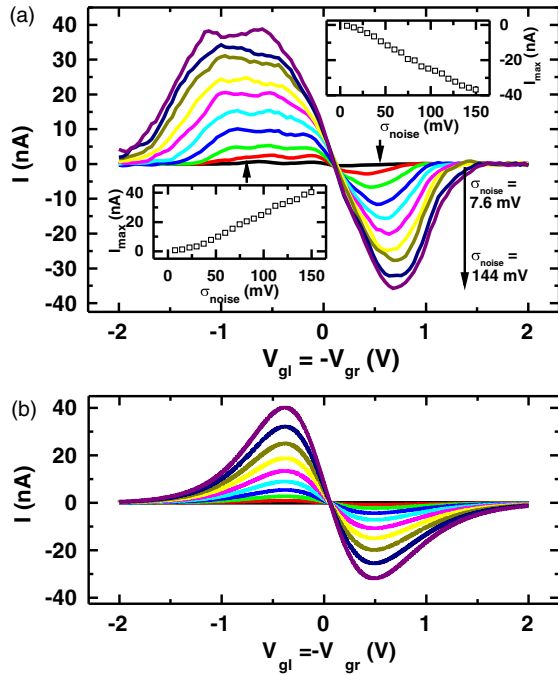
FIG. 3 (color online). (a) Experimental results of the noise rectification. The output current is plotted against $V_{gl} = -V_{gr}$ (push-pull) for noise amplitudes varied from 7.6 to 144 mV in steps of 15 mV. $V_{lr} = 0$ V, $V_{gb} = 4.7$ V. σ_{noise} controls the maximum current amplitude, while the side gates are able to influence the current flow's direction. The insets show the current maxima I_{max} in dependence on σ_{noise} up to 150 mV. (b) Simulated current rectification. I versus $V_{gl} = -V_{gr}$ (push-pull) for different noise amplitudes.

to the side gate efficiency for the left (right) gate. Thus, η_i accounts for the opening or closing of the channel via the gate voltage V_i. Following Ref. [27], the energy-dependent part of the conductance is modeled with $G'_i = (\partial/\partial V_i)G_i$. Inserting equations for G_i and G'_i for the rectification parameter and using the experimentally determined system parameters results in current-gate voltage traces as depicted in Fig. 3(b). These parameters are $T = 4.2$ K, $\eta_l = 0.12\%$, $\eta_r = 0.10\%$, $G_{\text{eff}} = e^2/h$, and $C_g/C_{\text{eff}} = 0.32$.

To harvest useful work from the device, it has to power a load or, equivalently, the generated current has to flow against a finite voltage difference. So, to measure the output power P, a voltage difference V_{lr} counteracting the current was applied between the channels. P is then given by $P = IV_{lr}$. Figures 4(a) and 4(c) show the measured powers P for both current directions plotted versus V_{lr}. The output power has a parabolic dependency on V_{lr} and vanishes at two particular points, one of them being at $V_{lr} = 0$ V and the other one occurring at the stopping voltage V_{st}, which depends on σ_{noise}. At $V_{lr} = V_{\text{st}}$, the generated current is compensated and I vanishes. The curves reach their maxima at half their corresponding stopping voltages.

In Figs. 4(a) and 4(c), σ_{noise} was varied from 7.6 to 150 mV. Increasing σ_{noise} results in an increase of both P_{max} and V_{st}. For $\sigma_{\text{noise}} = 150$ mV, the latter shifts up to -2.3 mV in the case of positive currents and up to 2.1 mV in the case of negative currents. Maximum output powers versus σ_{noise} are presented in Fig. 4(b) for positive and in

Fig. 4(d) for negative currents. Both curves show a quadratic dependency on the noise amplitude and reach maximal values of $P_{\text{max}} = 24$ pW and $P_{\text{max}} = 19$ pW, respectively.

In summary, we demonstrated a voltage fluctuation to current converter. The output current and power depend on the fluctuation's amplitude and reach maximum values in the nA and pW region, respectively. The demonstrated device is a major step to realizing efficient and sustainable electronics by means of energy harvesting in a well-known and widely applicable material system.

FIG. 4 (color online). (a) Output powers P versus V_{lr} for different σ_{noise} increasing from 7.6 to 150 mV in steps of 15 mV. $V_{\text{gl}} = -V_{\text{gr}} = -0.75$ V [cf. Fig. 3(a)]. The power curves feature a parabolic shape, are zero at $V_{lr} = 0$ V and at $V_{lr} = V_{\text{st}}$, and reach their maxima at $V_{lr} = V_{\text{st}}/2$. (b) Maximum output powers P_{max} against σ_{noise} at $V_{\text{gl}} = -V_{\text{gr}} = -0.75$ V. P_{max} exhibits a quadratic dependence on σ_{noise}. (c) Output powers P versus V_{lr} for different σ_{noise} increasing from 7.6 to 150 mV in steps of 15 mV. $V_{\text{gl}} = -V_{\text{gr}} = 0.55$ V. (d) Maximum output powers P_{max} against σ_{noise} at $V_{\text{gl}} = -V_{\text{gr}} = 0.55$ V. $V_{\text{gb}} = 4.7$ V for all figures. The side gate voltage configurations used here are displayed in Fig. 3 via two small black arrows.

*Corresponding author.
fabian.hartmann@physik.uni-wuerzburg.de
[1] H. Linke, T. E. Humphrey, A. Löfgren, A. O. Sushkov, R. Newbury, R. P. Taylor, and P. Omling, Science **286**, 2314 (1999).
[2] T. E. Humphrey and H. Linke, Phys. Rev. Lett. **94**, 096601 (2005).
[3] R. D. Astumian, Phys. Chem. Chem. Phys. **9**, 5067 (2007).
[4] P. Hänggi and F. Marchesoni, Rev. Mod. Phys. **81**, 387 (2009).
[5] R. D. Astumian and P. Hanggi, Phys. Today **55**, No. 11, 33 (2002).
[6] M. Büttiker, Z. Phys. B **68**, 161 (1987).
[7] R. Landauer, J. Stat. Phys. **53**, 233 (1988).
[8] A. Gnoli, A. Petri, F. Dalton, G. Pontuale, G. Gradenigo, A. Sarracino, and A. Puglisi, Phys. Rev. Lett. **110**, 120601 (2013).
[9] C. W. Chang, D. Okawa, A. Majumdar, and A. Zettl, Science **314**, 1121 (2006).
[10] N. Zeng and J.-S. Wang, Phys. Rev. B **78**, 024305 (2008).
[11] Z. L. Wang and J. Song, Science **312**, 242 (2006).
[12] Y. Qin, X. Wang, and Z. L. Wang, Nature (London) **451**, 809 (2008).
[13] S. Xu, B. J. Hansen, and Z. L. Wang, Nat. Commun. **1**, 93 (2010).
[14] R. Feynman, R. Leighton, and M. Sands, *The Feynman Lectures on Physics: Mainly Electromagnetism and Matter* (Addison-Wesley, Boston, 1965).
[15] L. W. Molenkamp, T. Gravier, H. van Houten, O. J. A. Buijk, M. A. A. Mabesoone, and C. T. Foxon, Phys. Rev. Lett. **68**, 3765 (1992).
[16] S. F. Godijn, S. Möller, H. Buhmann, L. W. Molenkamp, and S. A. van Langen, Phys. Rev. Lett. **82**, 2927 (1999).
[17] R. Scheibner, M. Knig, D. Reuter, A. D. Wieck, C. Gould, H. Buhmann, and L. W. Molenkamp, New J. Phys. **10**, 083016 (2008).
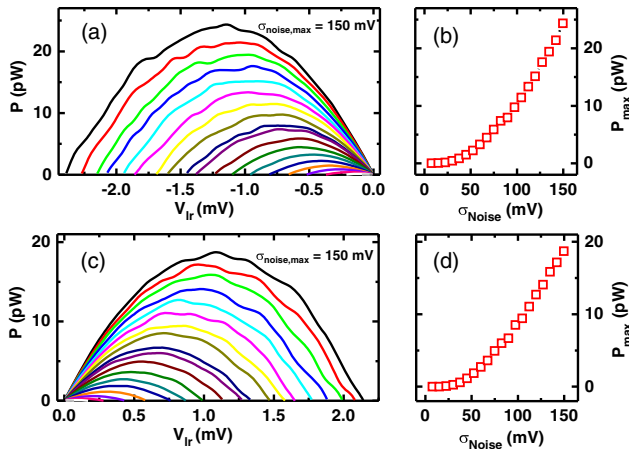[18] N. Nakpathomkun, H. Q. Xu, and H. Linke, Phys. Rev. B **82**, 235428 (2010).

[19] T. Ruokola and T. Ojanen, Phys. Rev. B **83,** 241404 (2011).

[20] S. Juergens, F. Haupt, M. Moskalets, and J. Splettstoesser, Phys. Rev. B **87,** 245423 (2013).

[21] D. Venturelli, R. Fazio, and V. Giovannetti, Phys. Rev. Lett. **110,** 256801 (2013).

[22] F. Haupt, M. Leijnse, H. L. Calvo, L. Classen, J. Splettstoesser, and M. R. Wegewijs, Phys. Status Solidi B **250,** 2315 (2013).

[23] M. Yamamoto, M. Stopa, Y. Tokura, Y. Hirayama, and S. Tarucha, Science **313,** 204 (2006).

[24] R. Sánchez, R. López, D. Sánchez, and M. Büttiker, Phys. Rev. Lett. **104,** 076801 (2010).

[25] D. Laroche, G. Gervais, M. Lilly, and J. Reno, Nat. Nanotechnol. **6,** 793 (2011).

[26] R. Sánchez and M. Büttiker, Phys. Rev. B **83,** 085428 (2011).

[27] B. Sothmann, R. Sánchez, A. N. Jordan, and M. Büttiker, Phys. Rev. B **85,** 205301 (2012).

[28] B. Sothmann, R. Sánchez, and A. N. Jordan, Nanotechnology **26,** 032001 (2015).

[29] S. Reitzenstein, L. Worschech, P. Hartmann, M. Kamp, and A. Forchel, Phys. Rev. Lett. **89,** 226804 (2002).

[30] C. Beenakker and H. van Houten, in *Semiconductor Heterostructures and Nanostructures*, Solid State Physics Vol. 44, edited by H. Ehrenreich and D. Turnbull (Academic Press, New York, 1991) pp. 1–228.